Stress-hardening behaviour of biofilm streamers

Giovanni Savorana[1], Tommaso Redaelli[1], Domenico Truzzolillo[2], Luca Cipelletti[2,3], Eleonora Secchi[1*]

[1*]Department of Civil, Environmental and Geomatic Engineering, ETH Zurich, Zurich, Switzerland.
[2]Laboratoire Charles Coulomb (L2C), Université Montpellier, Montpellier, France.
[3]Institut Universitaire de France, Paris, France.

*Corresponding author(s). E-mail(s): esecchi@ethz.ch;

Abstract

Bacteria's ability to withstand mechanical challenges is enhanced in their biofilm lifestyle, where they are encased in a viscoelastic polymer matrix [1]. Under fluid flow, biofilms can form as streamers – slender filaments tethered to solid surfaces and suspended in the flowing fluid [2, 3]. Streamers thrive in environments subjected to intense hydrodynamic stresses, such as medical devices and water filters, often resulting in catastrophic clogging [4]. Their colonisation success may depend on a highly adaptable mechanical response to varying stress conditions, though the evidence and underlying mechanisms of this adaptation remain elusive. Here, we demonstrate that biofilm streamers exhibit a stress-hardening behaviour, with both differential elastic modulus and effective viscosity increasing linearly with external stress. This stress-hardening is consistent across biofilms with different matrix compositions, formed by various bacterial species, and under diverse growth conditions. We further demonstrated that this mechanical response originates from the properties of extracellular DNA (eDNA) molecules [5], which constitute the structural backbone of the streamers. Our findings reveal an instantaneous, purely physical mechanism enabling streamers to adapt to hydrodynamic stresses. Given the ubiquity of eDNA in biofilms [1, 6], this discovery prompts a re-evaluation of its functional role in biofilm mechanics. Moreover, the stress-hardening behaviour may have broad implications for biofilm development, survival, and ecology, paralleling its role in tissues where it regulates processes such as morphogenesis, cancer formation and wound healing [7, 8].

Introduction

Biofilms are ubiquitous bacterial communities held together by a matrix of extracellular polymeric substances (EPS) [1, 9, 10]. Their ability to thrive in diverse environments is largely attributed to the EPS matrix's viscoelastic behaviour [11–15], which is also recognised as a virulence factor in biofilm-associated infections [12]. Protected by the matrix, the biofilm community responds to mechanical stresses from the environment through both biological and physical processes. On the one hand, mechanical stresses activate mechanosensing responses at the single-cell level, which in turn regulate EPS secretion [16, 17]. On the other hand, physical interactions between bacteria and their surroundings induce cellular ordering and shape the biofilm microstructure [18–20]. Additionally, preliminary studies suggest that biofilms may exhibit nonlinear rheological behaviours under stress [21–25]. However, it remains unclear whether and how biofilms can adjust their mechanical properties in response to environmental mechanical stresses.

Biofilms can successfully colonise environments ranging from medical devices to natural ecosystems, where flow velocities and hydrodynamic stresses can vary by several orders of magnitude

[13]. Notably, fluid flow promotes the formation of streamers [4, 26]. The formation and structural integrity of streamers rely entirely on the viscoelastic nature of the EPS matrix, which enables them to withstand hydrodynamic stresses and extend far from colonised surfaces, facilitating bacterial spreading [2, 3]. Streamer formation has been mainly studied in *Pseudomonas aeruginosa*, a key pathogen in chronic infections and antibiotic resistance, and a model organism for biofilm research [27–31]. In the PA14 strains, the main EPS components of streamers are extracellular DNA (eDNA), which constitutes their structural backbone, and the polysaccharide Pel, which influences their morphology and viscoelastic properties [2, 3]. eDNA provides structural integrity also to *P. aeruginosa* PAO1 and *Burkholderia cenocepacia* streamers [3, 32], indicating that it may serve a structural role across streamers formed by multiple species. Given that single DNA molecules exhibit stress-hardening behaviour — thus stiffen in response to increasing mechanical stress [5, 33] — it can be hypothesised that eDNA not only contributes to the structural integrity of streamers but also enhances their mechanical resilience.

In this work, we characterise biofilm streamers grown under a range of flow velocities to investigate how their viscoelastic properties change in response to the hydrodynamic stress exerted by the environment. We identify and model the primary mechanism driving their mechanical adaptation, which we found to be conserved across multiple bacterial species. Identifying biofilm adaptive mechanical response and uncovering its underlying mechanism advances our understanding of biofilm resilience in dynamic environments, offering novel perspectives on biofilm ecology and providing crucial insights for the development of more effective eradication strategies.

In situ characterisation of biofilm streamer viscoelasticity.

To systematically examine the viscoelasticity of biofilm streamers under different flow velocities, we use a microfluidic platform to grow streamers with a reproducible morphology and characterise their material properties *in situ* [2]. Pillar-shaped obstacles placed in a straight microfluidic channel act as nucleation points for pairs of biofilm streamers, which develop as millimetre-long filaments tethered to the sides of the pillars when a diluted bacterial suspension is flown through the channel. They grow over time, extending in the flow direction. Once they reach a stable morphology, we perform extensional rheological measurements on nearly cell-free portions of a streamer, thus determining the viscoelastic properties of homogeneous EPS matrix samples. Since streamers develop under continuous background flow, they are constantly subjected to an extensional axial stress σ and remain in a state of deformation with a non-zero extensional strain ε. The axial stress at position x along a streamer of total length L depends on the surface area of the downstream portion of the streamer exposed to flow and is expressed as:

$$\sigma\left(x\right) = \frac{1}{A(x)} \int_{x}^{L} \int_{0}^{2\pi} \left(\bar{\bar{\sigma}}(x',\,\theta) \cdot \hat{n}(x',\,\theta)\right) \cdot \hat{x}\, R(x')\, \mathrm{d}x'\, \mathrm{d}\theta, \tag{1}$$

where $A\left(x\right) = \pi R^2\left(x\right)$ is the cross-sectional area of the streamer at x, $\bar{\bar{\sigma}}$ is the Cauchy stress tensor of the fluid flowing past the streamer, $\hat{n}$ is the unit vector perpendicular to the streamer surface, and $\hat{x}$ is the unit vector in the x direction, parallel to the main axis of the streamer [2]. Equation 1 shows that the axial stress $\sigma(x)$, at a given position x along the streamer, depends not only on the stress tensor of the fluid $\bar{\bar{\sigma}}$, which is proportional to the flow velocity, but also on the morphology of the portion of streamer downstream of x. To test the viscoelastic properties of a streamer, we apply a controlled flow perturbation that imposes an increase in extensional stress $\Delta\sigma$ on top of the prestress σ_0 corresponding to the unperturbed flow velocity. This results in an additional filament deformation characterised by a strain increment $\Delta\varepsilon$. From these increments, we calculate the differential Young's modulus E_{diff} and effective viscosity η, quantifying the material properties of the streamer as a function of its prestress state σ_0. This differential testing method is analogous to the one implemented for characterising the shear rheology of cytoskeletal and extracellular biological networks in tissues [34, 35].

Ambient flow affects biofilm streamer morphology.

We investigate the adaptation of streamer morphology, biochemical composition, and viscoelasticity to different flow velocities U_{gr} using *P. aeruginosa* PA14. To investigate the role of polysaccharides

in the adaptation process, we compare PA14 strains with different levels of Pel polysaccharide production: the wild-type (wt) strain, which produces Pel in response to external forces [16, 17], the Pel-deficient mutant (Δpel) and the Pel-overproducer (ΔwspF), which is locked in the active state of Pel production [3].

Microfluidic experiments reveal that all *P. aeruginosa* PA14 strains form biofilm streamers across a range of flow velocities spanning an order of magnitude within the laminar regime ($\mathrm{Re} \in [0.02, 0.20]$, Extended Data Table 1). After 15 hours, streamers formed under different velocities exhibit similar morphologies but vary in average length L and radius R (Fig. 1e-f). These differences are due to flow-induced changes in cell and EPS assembly rather than biomass flux, which we maintain constant across conditions. The average length notably decreases with increasing flow velocity, regardless of Pel production levels (Fig. 1e). Time-lapse imaging shows that higher velocities delay the formation of the first stable biofilm threads, likely due to reduced cell attachment, consistent with observations on flat surfaces [36] (Extended Data Figure 1a, b). After the initial time lag t_0, the length increases with time approximately following a power law behaviour, $L \propto (t - t_0)^{0.5}$, under all flow conditions, with slower growth rates at higher velocities (Extended Data Figure 1c). Near the pillar (ROI_1, Fig. 1a, c), the radius increases significantly with flow velocity (Fig. 1f), while downstream (ROI_2, Fig. 1b, d), streamers are typically thinner, with the radius increasing with flow velocity for the wild-type strain, but showing no clear trends for the Pel-deficient and overproducer strains (Fig. 1f). Overall, these findings indicate that flow velocity significantly influences streamer development and morphology, with limited dependence on Pel polysaccharide abundance. It is important to highlight that the dependence of streamer morphology on ambient flow conditions implies that streamers grown at higher flow velocities are not necessarily subjected to higher extensional axial stresses, according to eq. 1.

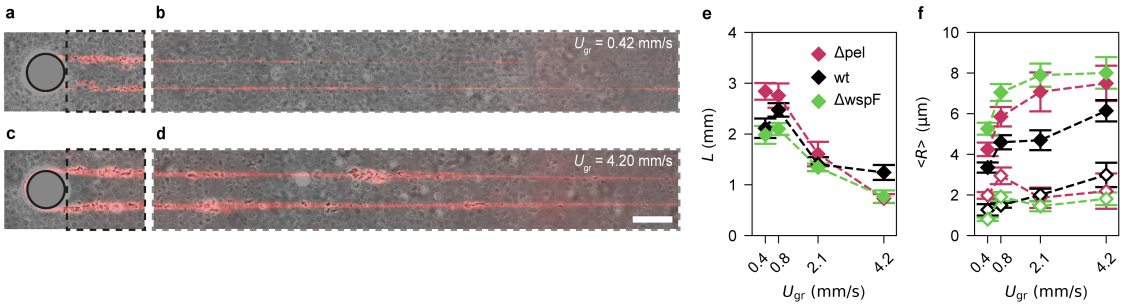

Fig. 1 The morphology of *P. aeruginosa* PA14 biofilm streamers is affected by ambient flow conditions during their growth. **a-d**, Representative overlaid phase contrast and fluorescence images of 15-h-old PA14 wild-type biofilm streamers grown on a micropillar at the lowest ($U_{\mathrm{gr}} = 0.42$ mm/s, **a**, **b**), and highest ($U_{\mathrm{gr}} = 4.20$ mm/s, **c**, **d**) average flow velocities tested in this study. The flow is laminar, and the flux of bacterial cells is constant across the different flow conditions. The black and grey dashed rectangles highlight the regions corresponding to ROI_1 ($x \in [25\ \mu\mathrm{m}, 125\ \mu\mathrm{m}]$) and ROI_2 ($x \in [400\ \mu\mathrm{m}, 1065\ \mu\mathrm{m}]$), respectively. The scale bar is 50 μm. Bacterial cells were imaged in phase contrast, and eDNA was stained using red-fluorescent propidium iodide (2 μg/mL). **e-f**, Average length L (**e**) and average of $\langle R \rangle$ in ROI_1 (**f**, closed symbols) and ROI_2 (**f**, open symbols) as a function of the average flow velocity U_{gr} inside the microchannel during streamer formation for PA14 Δpel (magenta), wild-type (black) and ΔwspF (green). The error bars are the standard error of the mean.

Rheological characterisation of streamers grown under different flow velocities.

Mechanical tests performed on PA14 biofilm streamers grown under different flow velocities show a linear relationship between the matrix viscoelastic properties and the axial stress exerted by fluid flow, revealing a strong mechanical adaptation mechanism of streamer viscoelasticity. We grow biofilm streamers for 15 hours at a constant flow velocity, and then we characterise the rheology of specific portions delimited by pairs of cell aggregates located at positions x_1 and x_2 within ROI_2. During the mechanical tests, we instantaneously double the initial flow velocity from $U_0 = U_{\mathrm{gr}}$ to $U_{\mathrm{cr}} = 2U_0$ (Extended Data Figure 2a). This increase results in a change in the average axial stress

on the examined portion of the streamer from the prestress value $\sigma_0 \equiv \langle \sigma(x; U_0) \rangle_{12}$ to the creep value $\sigma_{\mathrm{cr}} \equiv \langle \sigma(x; U_{\mathrm{cr}}) \rangle_{12}$, where the average is calculated between x_1 and x_2, and the notation $\sigma(x; U)$ explicitly shows the parametric dependence of the stress on flow velocity U. Neglecting fluid-structure interaction [2], we have $\sigma_{\mathrm{cr}} = 2\sigma_0$ (Extended Data Figure 2b). The corresponding stress increment $\Delta\sigma = \sigma_{\mathrm{cr}} - \sigma_0$ is maintained for 5 min, during which we use optical microscopy to quantify the time-dependent strain increment $\Delta\varepsilon\,(t)$ (Extended Data Figure 2c). Finally, we use $\Delta\sigma$ and $\Delta\varepsilon$ to determine the differential Young's modulus and effective viscosity of the sample portion under the prestress condition σ_0. Across a wide range of prestress conditions (Extended Data Figure 3), both the differential Young's modulus and effective viscosity exhibit an approximately linear correlation with the prestress ($E_{\mathrm{diff}} \propto \sigma_0^{0.99}$, $\eta \propto \sigma_0^{1.11}$) (Fig. 2).

The increase in differential Young's modulus with prestress maintains the elastic strain increment below 10% across all tested conditions (Extended Data Figure 5a). By restricting deformation and preserving the structure of bacterial communities under mechanical load, the stress-hardening behaviour may provide a competitive ecological advantage in dynamic ecosystems by keeping community members within interaction distance. Given the critical role of interactions within bacterial communities [37], further studies could reveal possible ecological implications.

We find that the observed linear dependence of the differential Young's modulus and effective viscosity on the prestress is independent of the EPS matrix composition in PA14 biofilm streamers. First, this trend is not determined by variations in eDNA density, which remains constant across a wide range of prestress conditions (Extended Data Figure 4). Second, the linear dependence observed in the PA14 Δpel strain indicates that this trend is not determined by Pel abundance. Nevertheless, Pel abundance influences the viscoelastic properties, as shown in previous work [2, 3]. For a given prestress value, the Pel-overproducer strain consistently displays a higher differential Young's modulus than both the Pel-deficient and the wild-type strains, which show similar values (Extended Data Figure 5b, c). Pel staining reveals that in the wild-type strain, significant amounts of Pel are detected only near the pillar (ROI_1 in Extended Data Fig. 6a-d) at higher flow velocities ($U_{\mathrm{gr}} = 2.10$ ml/h and $U_{\mathrm{gr}} = 4.20$ ml/h), while Pel concentration in the region where the mechanical properties are probed (ROI_2 in Extended Data Figure 6a-d) remains below our detection limit, regardless of flow velocity. Given that the viscoelastic properties of the EPS matrix correlate with the spatial distribution of polysaccharides within the biofilm [38], the similarity in the viscoelastic properties measured in both the wild-type and Pel-deficient mutants of the biofilm is consistent with the low levels of Pel polysaccharide found in the wild-type strain. In contrast, the ΔwspF mutant shows detectable Pel concentration in both ROI_1 and ROI_2 across all flow conditions, explaining its higher differential Young's modulus and effective viscosity compared to the other strains at a given prestress (Extended Data Figure 6e-h).

Given that the linear relationship between the viscoelastic properties and the prestress measured on streamers grown under different flow velocities cannot be attributed to flow-induced differences in EPS matrix composition, which are observed in surface-attached biofilms [19], we hypothesise that it may result from a nonlinear response of the matrix to mechanical stresses, as previously observed in eukaryotic biological networks formed from cytoskeletal and extracellular proteins [34, 35, 39]. To validate this hypothesis, each streamer must be tested under multiple prestress conditions.

Stress-hardening behaviour in PA14 biofilm streamers.

By testing the rheology of each streamer under multiple prestress conditions, we demonstrate that the linear dependence of the viscoelastic properties on prestress results from the stress-hardening behaviour of the EPS matrix. To conduct the tests, we first grow PA14 streamers at $U_{\mathrm{gr}} = 2.10$ mm/s for 15 h. After this growth period, we perform two sequential mechanical tests on each sample. The tests are conducted using different initial flow velocities U_0 for each test, with each U_0 having a corresponding creep velocity $U_{\mathrm{cr}} = 2U_0$. During the first test, the initial flow velocity is set to $U_0 = U_{\mathrm{gr}}$, which corresponds to a prestress of $\sigma_0 = \langle \sigma(x; U_{\mathrm{gr}}) \rangle_{12}$, as in the tests presented in the previous paragraph. After the first test, we decrease the flow velocity to $U_{\mathrm{gr}}/5 = 0.42$ mm/s and let the system stabilise for 10 minutes. Following this, we perform a second mechanical test with initial flow velocity $U_0 = U_{\mathrm{gr}}/5$, corresponding to a prestress $\sigma_0 = \langle \sigma(x; U_{\mathrm{gr}}/5) \rangle_{12}$ (Extended Data Figure 2). We image and analyse the same portion of the streamer in both tests to measure the differential Young's modulus and effective viscosity of the same sample under the two different

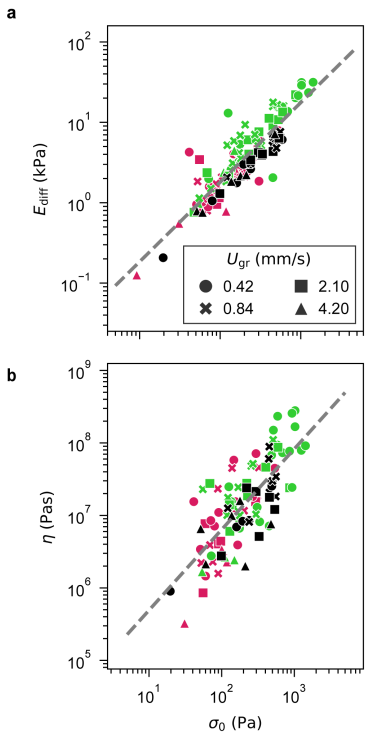

Fig. 2 The viscoelastic properties of *P. aeruginosa* PA14 biofilm streamers linearly depend on the prestess σ_0 exerted by U_{gr}. a, b, Differential Young's modulus E_{diff} and effective viscosity η as a function of prestress σ_0. Each point is measured on a portion of a different streamer, whose prestress value $\sigma_0 = \langle \sigma(x; U_{gr}) \rangle_{12}$ is determined by sample morphology and U_{gr}. All samples are tested after 15 h of growth. Different colours represent the different PA14 mutants: Δpel (magenta), wild-type (black), and ΔwspF (green). Different symbols represent data points obtained for samples grown at different average flow velocities U_{gr}: 0.42 mm/s (circles), 0.84 mm/s (crosses), 2.10 mm/s (squares) and 4.20 mm/s (triangles). The dashed grey lines are power-law fits of the data, with exponent 0.99 ± 0.05 ($R^2 = 0.79$) with a 95% confidence interval $[0.90, 1.08]$ in **a** and 1.11 ± 0.10 ($R^2 = 0.56$) with a 95% confidence interval $[0.92, 1.31]$ in **b**.

prestress conditions (Extended Data Figure 2d-f). In some selected experiments, we reverse the order of the mechanical tests to ensure that the observed viscoelastic properties are independent of the loading history, testing the streamer first under prestress $\sigma_0 = \langle \sigma(x; U_{gr}/5) \rangle_{12}$ and then under prestress $\sigma_0 = \langle \sigma(x; U_{gr}) \rangle_{12}$.

The differential Young's modulus and effective viscosity values measured sequentially on the same sample exhibit the same linear dependence on prestress as in streamers grown under different ambient flow conditions (Fig. 2, 3). This trend is consistent across all PA14 mutants, regardless of their Pel polysaccharide production levels, and is, therefore, independent of Pel abundance. The 10-minute interval between the tests is sufficient for the system to stabilise at the new flow velocity but too brief for bacteria to initiate any adaptive mechanisms [16]. Therefore, we conclude that the rheological adaptation of the streamer EPS matrix to the prestress is an instantaneous, purely physical stress-hardening response, which also explains the trends observed for streamers grown under different flow velocities (Fig. 2).

Given the dependence of viscoelastic properties on prestress, biofilm streamers should be compared based on tests conducted at a fixed prestress rather than a fixed flow velocity. This is demonstrated by the PA14 wild-type and Δpel streamers, which show no significant differences in the differential Young's modulus and effective viscosity when measured as a function of prestress but show apparent differences when results are aggregated by flow conditions (Extended Data Figure 5b, c) [2, 3].

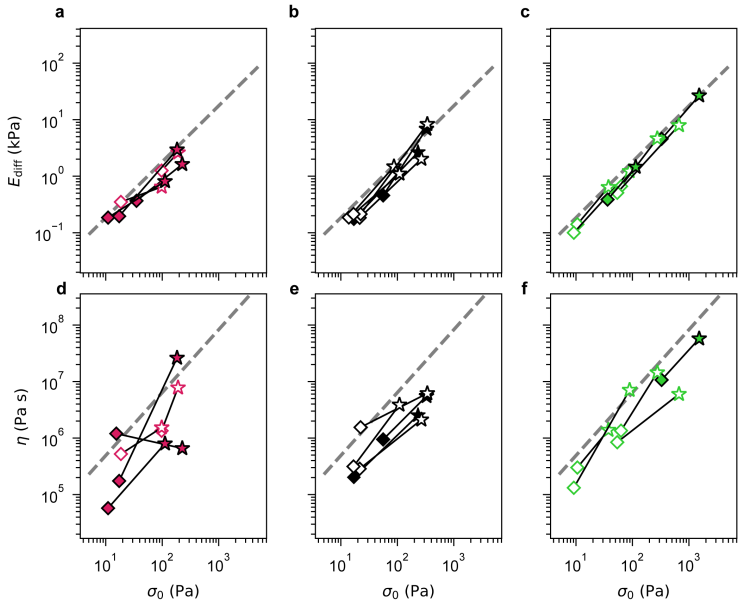

Fig. 3 The EPS matrix of *P. aeruginosa* PA14 biofilm streamers displays stress-hardening viscoelastic properties. Differential Young's moduli E_{diff} (**a-c**) and effective viscosities η (**d-f**) obtained from sequential mechanical tests demonstrate the stress-hardening behaviour of the matrix of PA14 Δpel (**a**, **d**, magenta), wild-type (**b**, **e**, black), and ΔwspF (**c**, **f**, green) streamers. Each pair of markers connected by a solid line represents values sequentially measured on a same sample under two different prestress conditions σ_0. The tests are conducted on PA14 biofilm streamers grown for 15 h at an average flow velocity $U_{\mathrm{gr}} = 2.10$ mm/s. The two tests performed on each sample are conducted with initial flow velocities $U_0 = U_{\mathrm{gr}} = 2.10$ mm/s (stars) and $U_0 = U_{\mathrm{gr}}/5 = 0.42$ mm/s (diamonds). The corresponding prestress values are $\sigma_0 = \langle \sigma(x; U_{\mathrm{gr}}) \rangle_{12}$ and $\sigma_0 = \langle \sigma(x; U_{\mathrm{gr}}/5) \rangle_{12}$. Open symbols mark data measured first at $U_0 = U_{\mathrm{gr}}$ and then at $U_0 = U_{\mathrm{gr}}/5$, while closed symbols are measured at $U_0 = U_{\mathrm{gr}}/5$ and then at $U_0 = U_{\mathrm{gr}}$. The dashed grey lines in **a-c** and **d-f** are the power law fits of the data reported in Fig. 2a and b, respectively. We verified that the observed strain-hardening behaviour is not significantly altered if fluid-structure interaction is accounted for in the calculation of the streamer rheology (Extended Data Fig. 9).

Stress-hardening behaviour in streamers across several bacterial species.

Experiments conducted with several widely spread bacterial species, common infection agents and model organisms for biofilm research, demonstrate that stress-hardening is a universal feature of the biofilm streamer EPS matrix. In these experiments, we grow streamers using suspensions of *P. aeruginosa* PAO1, *B. cenocepacia* H111, *S. epidermidis* 1457, and *E. coli* RP437, flowing at $U_{\mathrm{gr}} = 2.10$ mm/s for 15 h. These species differ in shape, motility and EPS components, with *S. epidermidis* being gram-positive and the others gram-negative bacteria [40–44]. Despite these differences, all species form biofilm streamers with an eDNA backbone, morphologically similar to those produced by PA14 (Fig. 4a-d).

Sequential mechanical tests performed under different prestress, as those in Fig. 3, reveal the same stress-hardening behaviour observed in PA14 streamers (Fig. 4e-h). Specifically, the differential Young's modulus of the streamers from all species scales linearly across a wide range of prestress, spanning nearly three orders of magnitude (Fig. 4i). Moreover, the prefactor also remains consistent across the testing conditions (Fig. 2 and Fig. 3) and different bacterial species (Fig. 4). The consistent stress-hardening behaviour and linear scaling observed across different species, combined with the presence of eDNA as a common and abundant component in their EPS matrices, suggests a link between this stress-hardening and the mechanical properties of the eDNA backbone.

Entropic elasticity as the origin of stress-hardening behaviour in streamers.

The stress-hardening behaviour of the differential elastic modulus of the streamers can be attributed to the entropic elasticity of their eDNA backbone. We demonstrate this by modelling the expected elastic response of a DNA network under uni-axial extension, using a framework based on the

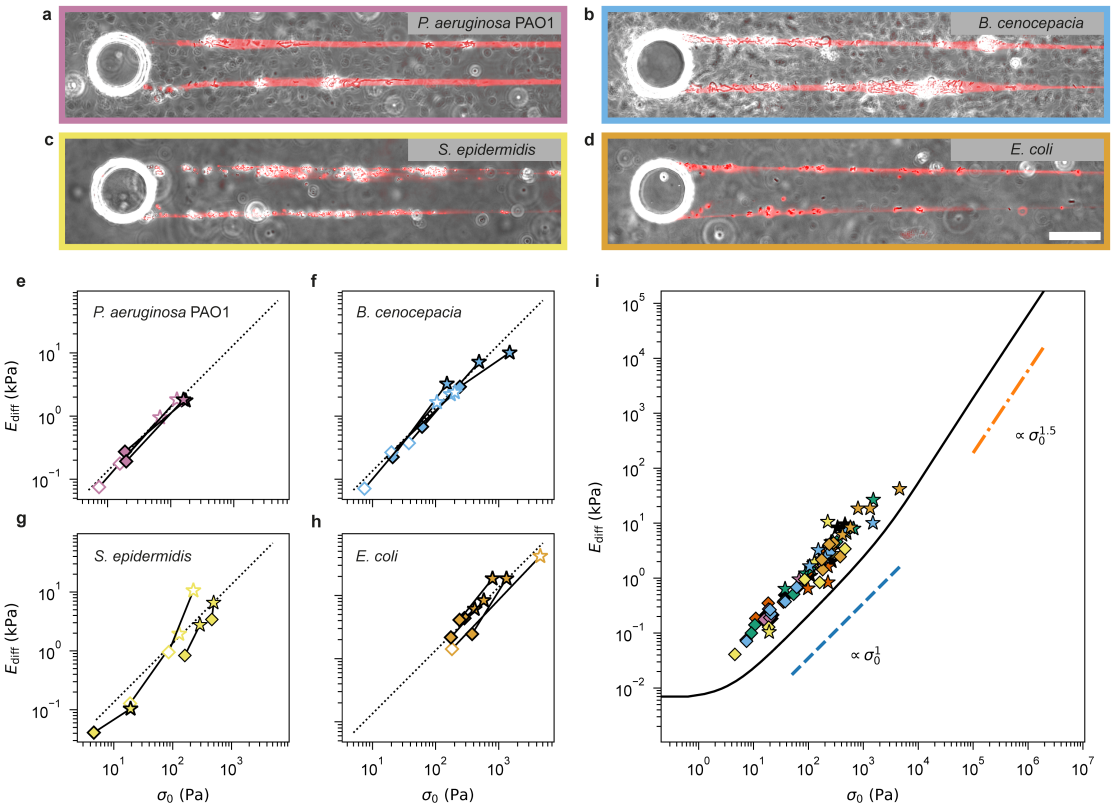

Fig. 4 The stress-hardening behaviour of the EPS matrix is consistent across biofilm streamers from several bacterial species. **a-d**, Representative overlaid phase contrast and fluorescence images of portions of biofilm streamers grown for 15 h at an average ambient flow velocity of $U_{\rm gr} = 2.10$ mm/s by *P. aeruginosa* PAO1 (**a**), *B. cenocepacia H111* (**b**), *S. epidermidis* 1457 (**c**), and *E. coli* RP437 (**d**). The scale bar is 50 µm. **e-h**, Differential Young's moduli $E_{\rm diff}$, obtained from sequential mechanical tests, as a function of the axial stress σ_0, demonstrating the stress-hardening behaviour of biofilm streamers formed by *P. aeruginosa* PAO1 (**e**), *B. cenocepacia* H111 (**f**), *S. epidermidis* 1457 (**g**), and *E. coli* RP437 (**h**), grown at average flow velocity $U_{\rm gr} = 2.10$ mm/s. Solid lines connect results from the same portion of the streamer tested under two axial stress conditions σ_0. Tests are conducted on 15-hour-old streamers with initial flow velocities $U_0 = U_{\rm gr} = 2.10$ mm/s (stars) and $U_0 = U_{\rm gr}/5 = 0.42$ mm/s (diamonds). The corresponding prestress values are $\sigma_0 = \langle \sigma(x; U_{\rm gr})\rangle_{12}$ and $\sigma_0 = \langle \sigma(x; U_{\rm gr}/5)\rangle_{12}$. Open symbols indicate data measured first at the higher and then lower values of σ_0, while closed symbols are measured at the lower and then at the higher values of σ_0. The dotted lines in panels **e-h** indicate a power law behaviour with exponent equal to 1. **i**, The black line shows the differential Young's modulus $E_{\rm diff}$ as a function of prestress σ_0 for a 3D network of worm-like chains under uni-axial extension, modelled using the eight-chain model [45]. The curve was calculated as explained in the Supplementary Information, assuming $T = 293$ K, $A = l = 50$ nm, $N = 1000$, $n = 10^{21}\, m^{-3}$. The scaling in the crossover regime at intermediate prestress, where $E_{\rm diff} \propto \sigma_0^1$, and in the high prestress regime, where $E_{\rm diff} \propto \sigma_0^{1.5}$, are indicated by dashed blue and dash-dotted orange lines, respectively. The markers show the data reported in panels **a-c** of Fig. 3 and panels **e-h** of this figure (same symbols and colour code of the original panels).

worm-like chain model [45], and the persistence length of DNA [5] (Supplementary Information). This model accounts for the entropic elasticity of DNA molecules and was previously applied to describe the strain-hardening behaviour in DNA gels under shear [5, 46]. In the uni-axial extension configuration tested in our experiments, the model predicts three regimes: a linear elastic regime at low prestress, where $E_{\rm diff}$ is constant, a crossover regime at intermediate prestress where $E_{\rm diff} \propto \sigma_0$, and a regime at large prestress where $E_{\rm diff} \propto \sigma_0^{1.5}$ (Fig. 4, i). Notably, this predicted crossover regime overlaps with the range of prestress observed in our experiments, assuming high DNA densities ($n \approx 10^{21}\, m^{-3}$) and a contour length of DNA chains between neighbouring cross-links $L_c \geq 50$ µm (Supplementary Information). The agreement in the linear scaling between prestress and the differential elastic modulus observed in both the experimental data and the model suggests that the stress-hardening behaviour of streamers originates from the entropic mechanical properties of eDNA. Further experimental characterisation of the internal structure of the eDNA network in streamers will likely improve the agreement between the prefactors. Additionally, while our

current modelling results focus on the differential elastic modulus, a more comprehensive model that includes the effective viscosity would be needed to fully capture the mechanical behaviour of streamers.

Conclusion

Although the colonisation success of biofilms in dynamic and challenging habitats suggested the presence of adaptive mechanical responses enhancing their resilience, direct evidence remained elusive. Here, we demonstrated a strong adaptation of biofilm streamer viscoelastic properties to varying mechanical stress conditions, driven by the stress-hardening behaviour of the biofilm matrix. Stress-hardening not only explains the ability of streamers to withstand rapid mechanical perturbations but also accounts for the difference in viscoelastic properties measured in samples grown under different flow velocities. Notably, this behaviour is consistent across multiple bacterial species, reflected in a linear dependence of the differential Young's modulus and extensional viscosity on the axial prestress exerted by fluid flow. This stress-hardening response is observed across a wide range of prestress values, spanning three orders of magnitude, suggesting its role as a highly effective adaptation mechanism in dynamic environments.

The strong agreement between the scaling observed in our experiments and the predicted elastic response of a DNA network under uniaxial extension indicates that the stress-hardening behaviour of streamers is entropic in nature, controlled by the mechanical properties of single DNA molecules, which form the backbone of streamers across all bacterial species tested in this study. Importantly, the scaling exponent relating viscoelasticity and axial prestress is independent of polysaccharides in the matrix, further underscoring the key role of eDNA in determining streamer viscoelasticity. Since the stress-hardening behaviour of single DNA molecules contributes to the overall stress-hardening of biofilm streamers, and eDNA is a widespread component of biofilms with diverse architectures [1, 6], it is crucial to reconsider and further investigate the functional role of eDNA in biofilm mechanics. Furthermore, we propose that this marked stress-hardening behaviour may have far-reaching implications for biofilm development and survival, much like the role of stress-hardening in tissues, where it preserves integrity and regulates processes such as morphogenesis and wound healing [7, 8].

Methods

Bacterial culture conditions

The following bacterial species are used in this study: *Pseudomonas aeruginosa* PA14 wild-type, the Pel deletion mutant PA14 ΔpelE, the Pel-overproducer PA14 ΔwspF, *Pseudomonas aeruginosa* PAO1 wild-type, *Burkholderia cenocepacia* H111, *Staphylococcus epidermidis* 1457 and *Escherichia coli* RP437. The *B. cenocepacia* suspensions are prepared according to [32] by inoculating cells from a frozen stock in 3 ml of ABC medium and incubating overnight at 37 °C while shaking at 200 rpm. 30 µl of the overnight suspension are then inoculated in 3 ml of ABC medium and incubated for 6 h at 37 °C while shaking at 200 rpm, until $OD_{600} = 0.3$ is reached. The overnight suspensions are then diluted in fresh Tryptone Broth (10 g/l tryptone, 5 g/l NaCl) to a final optical density $OD_{600} = 0.006$ and loaded into glass syringes. For all other bacterial species, suspensions are prepared by inoculating Luria broth 1.5% agar plates from frozen stocks and incubating them overnight at 37 °C. Cells from a single colony are inoculated in 3 ml of liquid medium and incubated at 37 °C for 3 h while shaking at 200 rpm, until $OD_{600} = 0.3$ is reached. M9 minimal medium (0.4% glucose) is used for *E. coli*, and Tryptone Broth (10 g/l tryptone, 5 g/l NaCl) is used for all other strains. The suspensions are then diluted in the respective fresh liquid media to a final optical density of $OD_{600} = 0.006$ and loaded into glass syringes.

Formation of biofilm streamers under different ambient flow conditions

Biofilm streamers are cultured and tested in the polydimethylsiloxane (PDMS) microfluidic platform described in [2]. Briefly, the platform consists of four straight channels with isolated micropillars that act as nucleation sites for pairs of biofilm streamers when a bacterial suspension is flown at a constant average flow velocity U_{gr}. The channels have width $W = 1\,\mathrm{mm}$, height

$H = 40\,\mu\text{m}$ and length $L = 4\,\text{cm}$. The cylindrical micropillars span the whole height of the channel, and their radius is $R_{\text{pillar}} = 25\,\mu\text{m}$. In this study, the number and locations of the micropillars within each microchannel are slightly modified from those of the original platform to enhance the efficiency of streamer formation. In the new configuration, five pillars are positioned at varying y-coordinates across the width of each channel (Extended Data Fig. 7c), rather than being aligned at the channel half-width as in the original configuration. Such a staggered arrangement ensures that the pillars intercept different flow lines without screening each other from the biomass in flow. Four laminar flow conditions are tested in parallel across different channels of the same microfluidic platform. The same bacterial batch is used in all channels to minimise biological variability. The average flow velocities U_{gr} span an order of magnitude, corresponding to Reynolds numbers Re ranging from 0.02 to 0.20 (Extended Data Table 1). The Reynolds number is calculated as $\text{Re} = \rho U_{\text{gr}} D/\mu$, where ρ is the density of water, D is the pillar diameter, and μ is the dynamic viscosity of water. Flow velocities are controlled by a syringe pump (neMESYS 290N, CETONI, Germany). To maintain a constant flux of cells across the four different flow conditions, two syringes are used for each microfluidic channel (Extended Data Fig. 7a): one to inject bacterial suspensions at a constant flow rate $Q_{\text{cells}} = 0.06$ ml/h and the other to inject growth medium at a flow rate Q_{medium}. The value of Q_{medium} is set so as to reach the desired total flow rate $Q_{\text{gr}} = Q_{\text{cells}} + Q_{\text{medium}}$ in each channel. In the channel with the lowest flow rate, only the first syringe is used, such that $Q_{\text{gr}} = Q_{\text{cells}}$. The values of Q_{gr} used in this study correspond to the average flow velocities $U_{\text{gr}} = Q/(HW)$ reported in Extended Data Table 1. The streams from the two syringes are joined by a Y connector (P-514, IDEX) located before the channel inlet. After the Y connector, a 2.5-mm-wide and 2.2-cm-long straight connector (from the LVF-KMM-06 kit, Darwin Microfluidics) is added to ensure complete sample homogenisation before entering the channel. In the *Wisteria floribunda* lectin staining experiments, a third syringe is added to introduce the lectin solution once the streamers are formed (Extended Data Fig. 7b). This is achieved by incorporating an additional Y connector (P-514, IDEX) before the channel inlet. A shut-off valve (P-732, IDEX) is mounted on the lectin flow line to allow the delayed mounting of the lectin syringe.

Characterisation of streamer composition and morphology

Streamer composition and morphology are characterised as described in [2]. Briefly, the biofilm matrix components are fluorescently stained and then imaged using epifluorescence microscopy. eDNA in the matrix is stained using propidium iodide (PI), which was added to both the bacterial suspension and the growth medium syringes to a final concentration of 2 µg/ml.

The red fluorescence signal of PI is acquired at half-height of the microchannel, and then binarised and processed to determine the morphology of the streamers according to [2]. Specifically, image processing provides the radius $R(x)$ and centre $C(x, y_c(x))$ of the streamers' cross sections as functions of the streamwise coordinate x. This data is then used to measure the streamers' lengths L and average radii $\langle R \rangle$ over ROI_1 and ROI_2. Data reported in Fig. 1e, f are the values of L and $\langle R \rangle$ averaged over about 10 experimental replicates for each strain and flow condition. The morphological characterisation from the PI signal, acquired right before each mechanical test, is also used to build 3D models of the streamers for the numerical calculation of the corresponding axial prestresses σ_0, following the protocol presented in [2]. Additionally, the average eDNA intensity reported in Extended Data Fig. 4 is calculated for each sample by averaging the PI signal between the initial positions x_1, x_2 of the cell aggregates tracked during the rheological tests as

$$< I_{\text{DNA}} >_{12} = \left(\int_{x_1}^{x_2} \int_{y_{\min}(x')}^{y_{\max}(x')} \mathrm{d}x' \, \mathrm{d}y' \right)^{-1} \int_{x_1}^{x_2} \int_{y_{\min}(x')}^{y_{\max}(x')} I_{\text{DNA}}(x', y') \, \mathrm{d}x' \, \mathrm{d}y'$$

where $y_{\min}(x) = C(x, y_c(x)) - R(x))$ and $y_{\max}(x) = C(x, y_c(x)) + R(x))$. The integrals were performed as discrete sums over the image pixels. Pel in the matrix of PA14 wild-type and ΔwspF was stained using GFP fluorescently labelled *Wisteria floribunda* lectin (WFL, FL-1351-2, Vector Laboratories). WFL is diluted in phosphate-buffered saline solution at 10 µ/ml concentration and loaded into a syringe. Endpoint measurements are performed on 15-h-old biofilm streamers by flowing WFL in the microchannels for 30 min before image acquisition in the GFP fluorescence

channel. The WFL syringes are mounted after $t = 15\,\mathrm{h}$ from the start of the experiment, preventing overnight degradation of WFL. Tests for quantifying Pel abundance with WFL are performed on streamers grown without PI to avoid interactions between the two stains. After imaging WFL, the WFL syringes are replaced with PI syringes to stain and quantify eDNA abundance. Phase contrast microscopy is used to image bacterial cells. The experiments are performed at ambient temperature ($T = 23\,^{\circ}\mathrm{C}$).

Characterisation of streamer growth

Streamer growth under different flow conditions U_{gr} is characterised using 24-h-long time-lapse acquisitions. Phase contrast and mCherry fluorescence images are acquired every 15 min. The length, L, as a function of time, is measured by tracking the streamer tip on the mCherry fluorescence channel. Analysis of these time series showed that the initial growth stages often involved significant detachment events. These events are defined as reductions in length L below a minimum threshold of $L_0 = 250\,\mu\mathrm{m}$. At later stages, streamers typically reach a more stable growth regime. The onset of this second regime is identified for each streamer by the time t_0 at which $L(t) > L_0$ for all subsequent time points $t > t_0$. The average growth speed as a function of time for the second regime (Extended Data Fig. 1d) is calculated as the derivative of the power law fit reported in Extended Data Fig. 1c. The length threshold L_0 is set to a value corresponding to a distance $10R_{\mathrm{pillar}}$ from the pillar. At this distance, the flow velocity magnitude matches its unperturbed value far from the pillar (relative difference $< 0.1\%$) (Extended Data Fig. 1a). This choice allows us to neglect phenomena occurring near the pillar, where biofilm-substrate adhesion and hydrodynamic interaction with the complex flow field play an important role. The average waiting time t^* for the first irreversible attachment event of dead cells or eDNA aggregates to the pillar is calculated from the PI signal on the pillar surface (Extended Data Fig. 1b). The waiting time in each experimental replicate is measured as the time at which the first irreversible attachment event of PI-stained biomass on the pillar is observed, with a minimum size threshold set to the bacterial cell size. Data reported in Extended Data Fig. 1b, c for t_0, t^* and $L - L(t_0)$ are averaged over about 15 streamers for each flow condition.

Rheological tests

The rheological characterisation of biofilm streamers grown under different ambient flow conditions is performed *in situ* with mechanical tests following the technique described in [2]. For each flow condition U_{gr}, the mechanical tests are conducted imposing a three-stage flow profile: an initial 2.5-minute stage at flow velocity $U_0 = U_{\mathrm{gr}}$, a 5-minute creep stage at $U_{\mathrm{cr}} = 2U_0 = 2U_{\mathrm{gr}}$, and a final 2.5-minute recovery stage at $U_{\mathrm{rec}} = U_0 = U_{\mathrm{gr}}$ (Extended Data Fig. 2a). The initial axial stress $\sigma\left(x; U_{\mathrm{gr}}\right)$ in each test is numerically calculated with a 3D COMSOL simulation solving the Navier-Stokes equations of flow at average velocity U_{gr} around a 3D model of the streamer. The model is built based on the morphology determined by the PI signal acquired before the beginning of the test at average flow velocity U_{gr}, as described in [2]. During the test, we acquire phase contrast images of the streamer in ROI_2 at 1 fps. The deformation of a portion of streamer delimited by two cell aggregates located at x_1 and x_2 is measured by tracking their relative distance $l_{12}\left(t\right) = x_2\left(t\right) - x_1\left(t\right)$ over time, providing the strain increment $\Delta\varepsilon\left(t\right) = \left(l_{12}\left(t\right) - l_{12}\left(0\right)\right)/l_{12}\left(0\right)$ (Extended Data Fig. 2c). The typical strain increment is well described by a Maxwell model, with an instantaneous elastic contribution $\Delta\varepsilon_{\mathrm{el}}$ and a viscous deformation $\Delta\varepsilon_{\mathrm{visc}}\left(t\right) = \dot{\varepsilon}\,t$ linearly dependent on time, where $\dot{\varepsilon}$ is the strain rate. The stress values averaged over the examined portion of streamer ($x \in [x_1, x_2]$) during the three stages of the test are: the prestress $\sigma_0 \equiv \langle\sigma\left(x; U_0\right)\rangle_{12}$ during the initial stage; the creep stress $\sigma_{\mathrm{cr}} \equiv \langle\sigma\left(x; U_{\mathrm{cr}}\right)\rangle_{12}$, during the creep stage; and the recovery stress $\sigma_{\mathrm{rec}} = \sigma_0$ (Extended Data Fig. 2b). The notation $\langle\cdot\rangle_{12}$ denotes the average between x_1 and x_2. The applied extensional stress increment is $\Delta\sigma = \sigma_{\mathrm{cr}} - \sigma_0$. Assuming negligible fluid-structure interaction, $\sigma_{\mathrm{rec}} = \sigma_0$ and the stress increment is $\Delta\sigma = \sigma_0$. Thus, the numerical estimate of σ_0 and the measurements of $\Delta\varepsilon_{\mathrm{el}}$ and $\dot{\varepsilon}$ allow the calculation of the differential Young's modulus $E_{\mathrm{diff}} = \Delta\sigma/\Delta\varepsilon_{\mathrm{el}}$ and effective viscosity $\eta = \Delta\sigma/\dot{\varepsilon}$ of the examined portion of streamer as a function of the applied extensional prestress σ_0.

To obtain meaningful estimates of E_{diff} and η, $\Delta\sigma$ has to be selected such that the sample's response is locally linear in a neighbourhood of σ_0. We verified that the choice $\Delta\sigma = \sigma_0$ satisfies this condition (Extended Data Fig. 8).

To test the stress-hardening behaviour of the matrix, streamers are grown at $U_{\text{gr}} = 2.10\,\text{mm/s}$ for 15 h. Each sample undergoes two sequential mechanical tests, each at a different initial flow velocity U_0 and corresponding creep velocity $U_{\text{cr}} = 2U_0$. The first test is performed at $U_0 = U_{\text{gr}} = 2.10\,\text{mm/s}$, corresponding to a prestress $\sigma_0 = \langle\sigma(x; U_{\text{gr}})\rangle_{12}$. After the first test, the flow velocity is decreased to $U_{\text{gr}}/5 = 0.42\,\text{mm/s}$, and the system is allowed to stabilise for 10 minutes. The second test is then performed at $U_0 = U_{\text{gr}}/5 = 0.42\,\text{mm/s}$, corresponding to a presetress $\sigma_0 = \langle\sigma(x; U_{\text{gr}}/5)\rangle_{12} < \langle\sigma(x; U_{\text{gr}})\rangle_{12}$ (Extended Data Fig. 2d). Before each test, the PI signal is acquired to characterise the morphology of the streamer at the corresponding U_0. These morphologies are then used to numerically calculate the corresponding axial stresses with 3D COMSOL simulations, according to [2]. During two sequential tests on the same streamer, the relative distance $l_{12}(t)$ between the same pair of cell aggregates is tracked. This allows the quantification of E_{diff} and η of the same portion of streamer at the two different prestress values.

To estimate the effect of fluid-structure interaction (FSI) on the correlation between E_{diff} and σ_0 (Extended Data Fig. 9), we applied the iterative scheme presented in [2] to the dataset reported in Fig. 3b. The scheme is arrested at the first iteration since higher-order iterations have a negligible effect on the FSI correction, as shown by data reported in [2].

Acknowledgements. We thank Dr. Sam Charlton and Dr. Steffen Geisel for the insightful discussions, Ela Burmeister for the technical support, and support from the Swiss National Science Foundation PRIMA Grant 179834 (to E.S.). Finally, we acknowledge and honour the memory of Prof. Paul Stoodley, whose pioneering work in streamer formation and rheology has greatly influenced and inspired this research.

References

[1] Flemming, H.-C. & Wingender, J. The biofilm matrix. *Nat. Rev. Microbiol.* **8**, 623–633 (2010).

[2] Savorana, G., Słomka, J., Stocker, R., Rusconi, R. & Secchi, E. A microfluidic platform for characterizing the structure and rheology of biofilm streamers. *Soft Matter* **18**, 3878–3890 (2022).

[3] Secchi, E. *et al.* The structural role of bacterial eDNA in the formation of biofilm streamers. *Proc. Natl. Acad. Sci. U.S.A.* **119**, e2113723119 (2022).

[4] Drescher, K., Shen, Y., Bassler, B. L. & Stone, H. A. Biofilm streamers cause catastrophic disruption of flow with consequences for environmental and medical systems. *Proc. Natl. Acad. Sci. U.S.A.* **110**, 4345–4350 (2013).

[5] Bustamante, C., Marko, J. F., Siggia, E. D. & Smith, S. Entropic elasticity of lambda-phage DNA. *Science* **265**, 1599–1600 (1994).

[6] Whitchurch, C. B., Tolker-Nielsen, T., Ragas, P. C. & Mattick, J. S. Extracellular DNA required for bacterial biofilm formation. *Science* **295**, 1487–1487 (2002).

[7] Wyatt, T., Baum, B. & Charras, G. A question of time: tissue adaptation to mechanical forces. *Curr. Opin. Cell Biol.* **38**, 68–73 (2016).

[8] Corominas-Murtra, B. & Petridou, N. I. Viscoelastic networks: forming cells and tissues. *Front. Phys.* **9** (2021).

[9] Watnick, P. & Kolter, R. Biofilm, city of microbes. *J. Bacteriol.* **182**, 2675–2679 (2000).

[10] O'Toole, G., Kaplan, H. B. & Kolter, R. Biofilm formation as microbial development. *Annu. Rev. Microbiol.* **54**, 49–79 (2000).

[11] Peterson, B. W. *et al.* Viscoelasticity of biofilms and their recalcitrance to mechanical and chemical challenges. *FEMS Microbiol. Rev.* **39**, 234–245 (2015).

[12] Gloag, E. S., Fabbri, S., Wozniak, D. J. & Stoodley, P. Biofilm mechanics: Implications in infection and survival. *Biofilm* **2**, 100017 (2020).

[13] Caldara, M., Belgiovine, C., Secchi, E. & Rusconi, R. Environmental, microbiological, and immunological features of bacterial biofilms associated with implanted medical devices. *Clin. Microbiol. Rev.* **35**, e0022120 (2022).

[14] Persat, A. *et al.* The mechanical world of bacteria. *Cell* **161**, 988–997 (2015).

[15] Charlton, S. G. V. *et al.* Regulating, measuring, and modeling the viscoelasticity of bacterial biofilms. *J. Bacteriol.* **201**, 10.1128/jb.00101–19 (2019).

[16] Rodesney, C. A. *et al.* Mechanosensing of shear by *Pseudomonas aeruginosa* leads to increased levels of the cyclic-di-GMP signal initiating biofilm development. *Proc. Natl. Acad. Sci. U.S.A.* **114**, 5906–5911 (2017).

[17] Hickman, J. W., Tifrea, D. F. & Harwood, C. S. A chemosensory system that regulates biofilm formation through modulation of cyclic diguanylate levels. *Proc. Natl. Acad. Sci. U.S.A.* **102**, 14422–14427 (2005).

[18] Pearce, P. *et al.* Flow-induced symmetry breaking in growing bacterial biofilms. *Phys. Rev. Lett.* **123**, 258101 (2019).

[19] Hartmann, R. *et al.* Emergence of three-dimensional order and structure in growing biofilms. *Nat. Phys.* **15**, 251–256 (2019).

[20] Zhang, Q. *et al.* Morphogenesis and cell ordering in confined bacterial biofilms. *Proc. Natl. Acad. Sci. U.S.A.* **118**, e2107107118 (2021).

[21] Stoodley, P., Cargo, R., Rupp, C. J., Wilson, S. & Klapper, I. Biofilm material properties as related to shear-induced deformation and detachment phenomena. *J. Ind. Microbiol. Biotechnol.* **29**, 361–367 (2002).

[22] Grumbein, S., Werb, M., Opitz, M. & Lieleg, O. Elongational rheology of bacterial biofilms *in situ*. *J. Rheol.* **60**, 1085–1094 (2016).

[23] Wilking, J. N., Angelini, T. E., Seminara, A., Brenner, M. P. & Weitz, D. A. Biofilms as complex fluids. *MRS Bull.* **36**, 385–391 (2011).

[24] Jana, S. *et al.* Nonlinear rheological characteristics of single species bacterial biofilms. *npj Biofilms Microbiomes* **6**, 19 (2020).

[25] Zhang, Q. *et al.* Mechanical resilience of biofilms toward environmental perturbations mediated by extracellular matrix. *Adv. Funct. Mater.* **32**, 2110699 (2022).

[26] Rusconi, R., Lecuyer, S., Autrusson, N., Guglielmini, L. & Stone, H. A. Secondary flow as a mechanism for the formation of biofilm streamers. *Biophys. J.* **100**, 1392–1399 (2011).

[27] Moradali, M. F., Ghods, S. & Rehm, B. H. A. *Pseudomonas aeruginosa* lifestyle: A paradigm for adaptation, survival, and persistence. *Front. Cell. Infect. Microbiol.* **7**, 39 (2017).

[28] Ciofu, O., Moser, C., Jensen, P. Ø. & Høiby, N. Tolerance and resistance of microbial biofilms. *Nat. Rev. Microbiol.* **20**, 621–635 (2022).

[29] Jennings, L. K. *et al.* Pel is a cationic exopolysaccharide that cross-links extracellular DNA in the *Pseudomonas aeruginosa* biofilm matrix. *Proc. Natl. Acad. Sci. U.S.A.* **112**, 11353–11358

(2015).

[30] Friedman, L. & Kolter, R. Two genetic loci produce distinct carbohydrate-rich structural components of the *Pseudomonas aeruginosa* biofilm matrix. *J. Bacteriol.* **186**, 4457–4465 (2004).

[31] Friedman, L. & Kolter, R. Genes involved in matrix formation in *Pseudomonas aeruginosa* PA14 biofilms. *Mol. Microbiol.* **51**, 675–690 (2004).

[32] Heredia-Ponce, Z. *et al.* Genotoxic stress stimulates eDNA release via explosive cell lysis and thereby promotes streamer formation of *Burkholderia cenocepacia* H111 cultured in a microfluidic device. *npj Biofilms Microbiomes* **9**, 96 (2023).

[33] Marko, J. F. & Siggia, E. D. Stretching DNA. *Macromolecules* **28**, 8759–8770 (1995).

[34] Gardel, M. L. *et al.* Elastic behavior of cross-linked and bundled actin networks. *Science* **304**, 1301–1305 (2004).

[35] Licup, A. J. *et al.* Stress controls the mechanics of collagen networks. *Proc. Natl. Acad. Sci. U.S.A.* **112**, 9573–9578 (2015).

[36] Lecuyer, S. *et al.* Shear stress increases the residence time of adhesion of *Pseudomonas aeruginosa*. *Biophys. J.* **100**, 341–350 (2011).

[37] Alma, D. C., Simon, v. V., Daniel, J. K., Susan, S. & Martin, A. Short-range interactions govern the dynamics and functions of microbial communities. *Nat. Ecol. Evol.* **4**, 165–172 (2020).

[38] Ohmura, T. *et al.* In vivo microrheology reveals local elastic and plastic responses inside 3D bacterial biofilms. *Adv. Mater.* 2314059 (2024).

[39] Storm, C., Pastore, J. J., MacKintosh, F. C., Lubensky, T. C. & Janmey, P. A. Nonlinear elasticity in biological gels. *Nature* **435**, 191–194 (2005).

[40] Colvin, K. M. *et al.* The Pel polysaccharide can serve a structural and protective role in the biofilm matrix of *Pseudomonas aeruginosa*. *PLoS Pathog.* **7**, 1–13 (2011).

[41] Novotny, L. A., Amer, A. O., Brockson, M. E., Goodman, S. D. & Bakaletz, L. O. Structural stability of *Burkholderia cenocepacia* biofilms is reliant on edna structure and presence of a bacterial nucleic acid binding protein. *PloS One* **8** (2013).

[42] Chiarini, L. *et al.* Exopolysaccharides produced by *Burkholderia cenocepacia* reca lineages iiia and iiib. *J. Cyst. Fibros.* **3**, 165–172 (2004).

[43] Schilcher, K. & Horswill, A. R. Staphylococcal biofilm development: Structure, regulation, and treatment strategies. *Microbiol. Mol. Biol. Rev.* **84**, 10.1128/mmbr.00026–19 (2020).

[44] Hufnagel, D. A., Depas, W. H. & Chapman, M. R. The biology of the *Escherichia coli* extracellular matrix. *Microbiol. Spectr.* **3** (2015).

[45] Ogden, R. W., Saccomandi, G. & Sgura, I. On worm-like chain models within the three-dimensional continuum mechanics framework. *Proc. R. Soc. A: Math. Phys. Eng. Sci.* **462**, 749–768 (2006).

[46] Orakdogen, N., Erman, B. & Okay, O. Evidence of strain hardening in dna gels. *Macromolecules* **43** (2010).

Extended Data

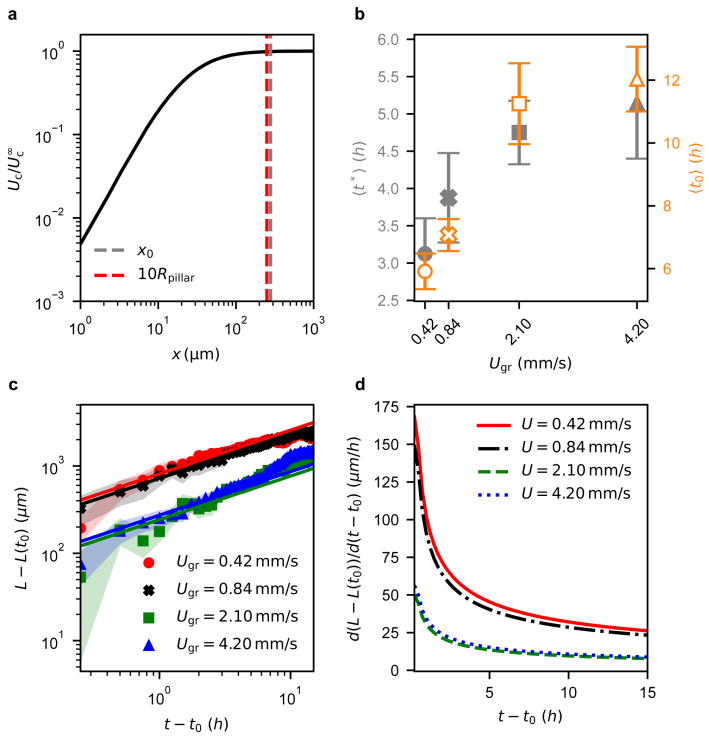

Extended Data Fig. 1 Effects of flow on the time scale of streamer inception and growth speed. **a**, Flow velocity magnitude U_c on the centerline of the microchannel as a function of the distance x from the pillar in the absence of streamers. The flow field was numerically calculated with a 3D COMSOL simulation of a pillar located at half-width of the channel. The dashed grey line indicates the distance x_0 where the relative difference between U_c and the unperturbed value U_c^∞ becomes less than 1%. The dashed red line shows that this position approximately corresponds to $10R_{\text{pillar}}$. **b**, Average waiting time t^* for the first irreversible attachment event of PI-stained cells or eDNA aggregates on the pillar (closed grey markers, left-hand y-axis) and time t_0 needed to observe a stable filament growing without major detachment events defined as drops of L below L_0 (open orange markers, right-hand y-axis). **c**, Averages of $L(t - t_0) - L(t_0)$ as a function of time in the stable growth regime ($t > t_0$) for the four different flow conditions tested in this study. $L(t)$ curves measured for single streamers were averaged from t_0 onwards after subtracting the value $L(t_0)$. This method excluded the initial stages of streamer formation, where major detachment events occur. The solid lines show best fits with $(t - t_0)^{0.5}$. **d**, Average growth speeds as a function of time for the different flow conditions, obtained as the time derivative of the fitting curves in **c**. The average growth speeds at $t = 15$ h are lower than 50 μm/h in all flow conditions,. Therefore, streamer growth is negligible during the time scale of the rheological tests (~ 10 min).

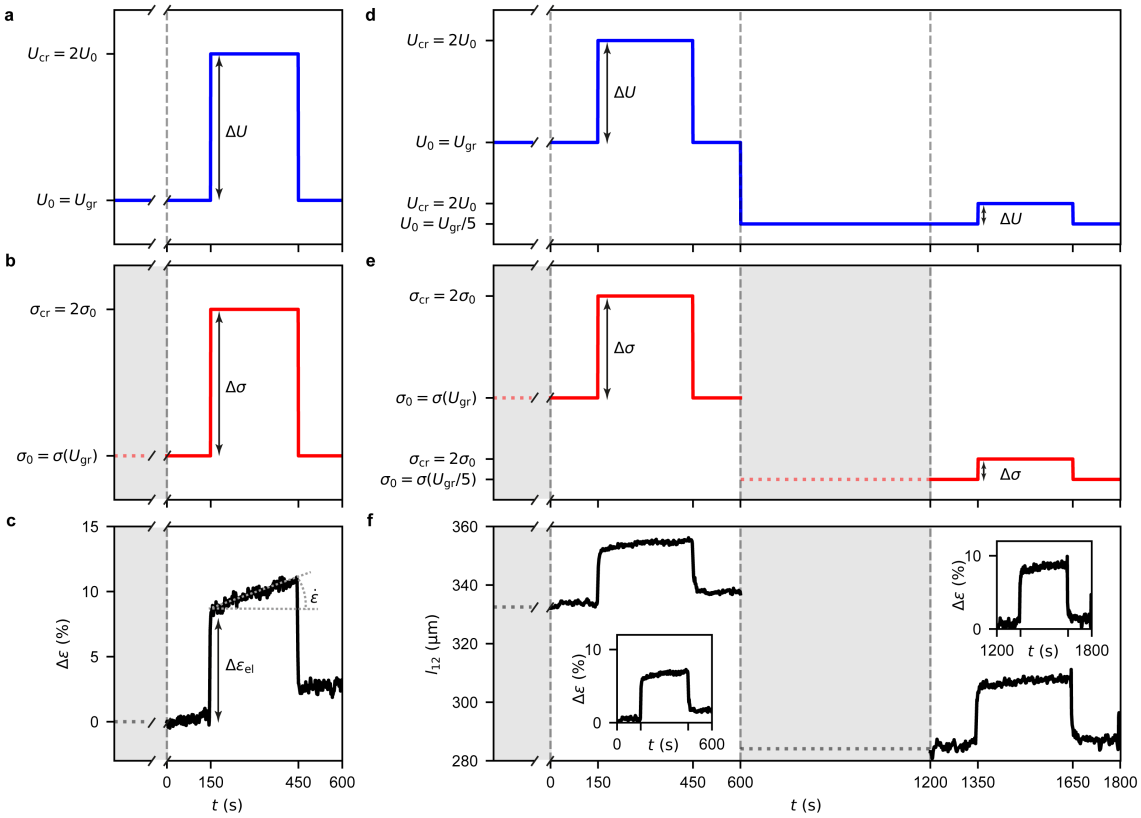

Extended Data Fig. 2 Mechanical test scheme. **a-c**, Average flow velocity U, axial stress σ and typical strain increment $\Delta\varepsilon$ of a streamer portion as a function of time t during the 10-min mechanical tests for the characterisation of biofilm streamers grown under different ambient flow conditions U_{gr} (Fig. 2) . **a**, In the 2.5-min initial stage of the test, the flow velocity is $U_0 = U_{gr}$; in the 5-min creep stage $U_{cr} = 2U_0 = 2U_{gr}$; in the 2.5-min recovery stage, U is decreased to the initial value $U_{rec} = U_0 = U_{gr}$. The dimension line shows the velocity increment ΔU imposed during the creep stage. The broken axis shows that the initial flow velocity U_0 equals the average flow velocity U_{gr}, maintained constant during streamer formation. **b**, The prestress σ_0 applied to the tested portion of the streamer during the initial stage corresponds to the axial stress exerted by flow at U_{gr}: $\sigma_0 = \langle\sigma(x; U_{gr})\rangle_{12}$. The doubling of the flow velocity during the creep stage corresponds to doubling the axial stress $\sigma_{cr} = 2\sigma_0$, if fluid-structure interaction is neglected. In the recovery stage of the test, the axial stress decreases to its initial value: $\sigma_{rec} = \sigma_0$. The dimension line shows the stress increment $\Delta\sigma = \sigma_{cr} - \sigma_0$ imposed during the creep stage. The axial stress before the beginning of the test (shaded region) is not determined: $\sigma(x; U_0)$ was characterised with 3D COMSOL simulations based on the PI fluorescence signal acquired before the test, at $t = 0$. **c**, The strain increment $\Delta\varepsilon(t)$ of the examined portion of streamer is well described by a Maxwell model, with an instantaneous elastic contribution $\Delta\varepsilon_{el}$ at $t = 150$ s and an irreversible time-dependent viscous deformation with strain rate $\dot{\varepsilon}$, which takes place during the creep stage of the test. When the axial stress increment is removed ($t = 450$ s), only the elastic deformation is recovered. The streamer portion is delimited by two cell aggregates, and its deformation is characterised by tracking their relative distance $l_{12}(t)$ on phase contrast images acquired at 1 fps, yielding the strain increment as $\Delta\varepsilon(t) = (l_{12}(t) - l_{12}(0))/l_{12}(t)$. **d-f**, Average flow velocity U, axial stress σ and typical length l_{12} of a streamer portion as a function of time t during two sequential mechanical tests (Fig. 3, Fig. 4). **d**, After 15 h of growth, a first 10-min mechanical test like the one represented in panels **a-c** is performed on a streamer at $U_0 = U_{gr}$ ($t \in [0, 600\,\text{s}]$). After the first test, the flow velocity is decreased to $U = U_{gr}/5$. After waiting 10 min for stabilisation, a second 10-min test is performed at $U_0 = U_{gr}/5$ ($t \in [1200\,\text{s}, 1800\,\text{s}]$). The corresponding average velocities during the creep and recovery stages during the second test are $U_{cr} = 2U_0 = 2U_{gr}/5$ and $U_{cr} = U_0 = U_{gr}/5$, respectively. **e**, Stress values applied to the same portion of streamer during the sequential tests. In the first and second tests, the applied prestresses are $\sigma_0 = \langle\sigma(x; U_{gr})\rangle_{12}$ and $\sigma_0 = \langle\sigma(U_{gr}/5)\rangle_{12}$, respectively. The prestress values are numerically calculated with 3D COMSOL simulations based on the PI fluorescence signal acquired before each test, at $t = 0$ and $t = 1200$ s. Since the two morphologies differ, $\sigma(x; U_{gr}/5) \neq \sigma(x; U_{gr})/5$. **f**, Typical length $l_{12}(t)$ of the portion of streamer delimited by the two cell aggregates tracked during the two tests, measured as explained in **c** during the first ($t \in [0, 600\,\text{s}]$) and the second test ($t \in [1000\,\text{s}, 1800\,\text{s}]$). The insets show the corresponding strain increments $\Delta\varepsilon$.

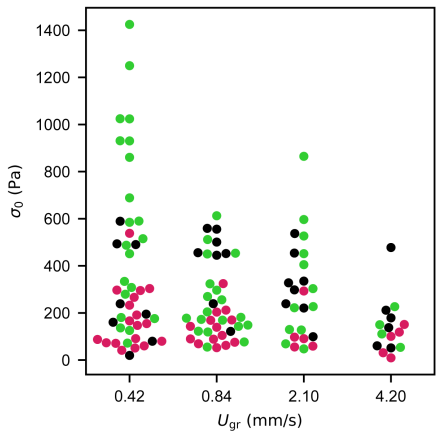

Extended Data Fig. 3 Distributions of prestress values σ_0 corresponding to the flow velocities U_{gr} tested in this study. The swarm plot illustrates the axial prestress values σ_0 exerted on the tested portion of each sample reported in Fig. 2. The axial stress corresponds to the prestress exerted by the background flow with average velocity U_{gr} on the examined portion of streamer during the 2.5-min initial stage of the rheological test. The swarm plot reports data for PA14 Δpel (magenta), wild-type (black), and ΔwspF (green). Since σ_{gr} is determined both by U_{gr} and streamer morphology, while it is true that streamers grown at a higher ambient flow condition are subjected to higher shear stresses and pressure gradients, it cannot be assumed that they are also subjected to higher axial stresses. This is clearly demonstrated at $U_{gr} = 4.20$ mm/s, the maximum U_{gr} tested. Despite being associated with the highest average shear stress and pressure gradient values, it exhibits the lowest average σ_0. This observation can be explained in light of the streamer morphology under this flow condition: lengths are shortest, and radii are widest (Fig. 1e-f), which decreases the overall axial stress on the streamer.

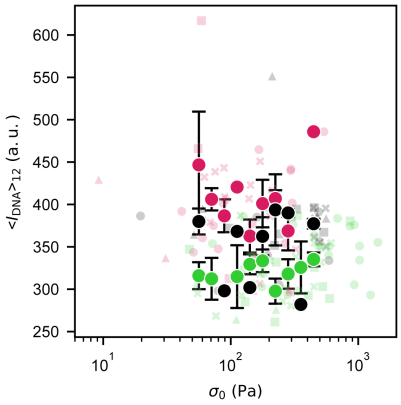

Extended Data Fig. 4 Average eDNA intensity I_{DNA} on the tested portion of streamer as a function of the applied prestress σ_0. Semitransparent symbols show the intensity of the eDNA fluorescence signal I_{DNA} averaged over the length of each tested portion of streamer reported in Fig. 2, as a function of the applied prestress $\sigma_0 = \langle \sigma\,(x; U_{\mathrm{gr}})\rangle_{12}$. Each value of $\langle I_{\mathrm{DNA}}\rangle_{12}$ was calculated between the positions x_1 and x_2 of the cell aggregates tracked during the stress test, as explained in the Methods. The different colours represent the different PA14 mutants: Δpel (magenta), wild-type (black) and ΔwspF (green). The different symbols represent data points obtained for samples grown at different average flow velocities U_{gr}: 0.42 mm/s (circles), 0.84 mm/s (crosses), 2.10 mm/s (squares) and 4.20 mm/s (triangles). Fully opaque markers were calculated by binning and averaging the semi-transparent points for each bacterial strain within 10 intervals of σ_0. These bins have equal width on a logarithmic scale and cover the stress range where data was collected for all the mutants. The error bars show the standard error of the mean.

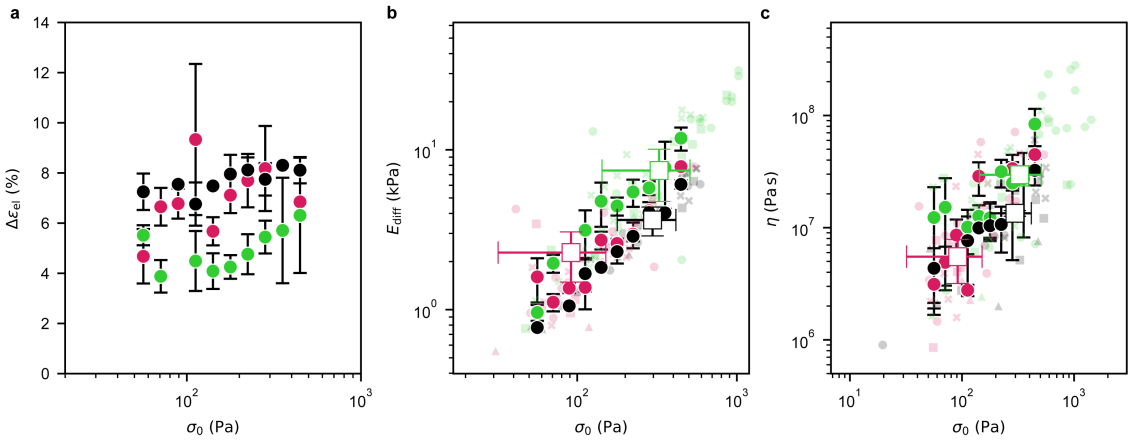

Extended Data Fig. 5 Pel abundance determines inter-strain rheological differences. **a**, Elastic contribution $\Delta\varepsilon_{\mathrm{el}}$ to the strain increment for the three strains, binned and averaged within 10 intervals of σ_0 (filled circles), as in Extended Data Fig. 4. The different colours represent the different PA14 mutants: Δpel (magenta), wild-type (black) and ΔwspF (green). The error bars are the standard error of the mean. This plot shows that the strain increment is independent of $\Delta\sigma/\sigma_0$. **b**,**c**, Semitransparent markers show the raw data reported in Fig. 2. Fully opaque markers represent values of E_{diff} (**b**) and η (**c**) binned and averaged as in panel **a**. The colour code is the same as in panel **a**, and the error bars are the standard error of the mean. Data show that, within a given axial stress interval, the Pel-overproducer strain ΔwspF displays significantly higher values of E_{diff}, while the Pel-deficient Δpel strain and the wild-type have comparable values within the statistical significance of our dataset (**b**). The same trend generally holds for η (**c**). The open square symbols represent the average values for streamers grown at $U_{\mathrm{gr}} = 2.1$ mm/s. The error bars are the standard error of the mean. Different edge colours correspond to different mutants, following the same colour code as above. The data show that wild-type and ΔwspF grown at $U_{\mathrm{gr}} = 2.1$ mm/s are subjected to approximately the same average axial stresses. Thus, the differences in E_{diff} and η cannot be attributed to the stress hardening behaviour but rather to differences in Pel abundance (Extended Data Fig. 6). In the case of the Δpel mutant, the average axial stress is significantly lower than those of the other strains. This observation suggests that the differences between the average values measured for the wild-type and Δpel mutants result mainly from the stress-hardening behaviour when testing streamers at a fixed U rather than at fixed σ. In light of these results, we can conclude that there are no significant rheological differences between the Δpel and wild-type matrices at fixed σ_0, in agreement with composition results reported in Extended Data Fig. 6.

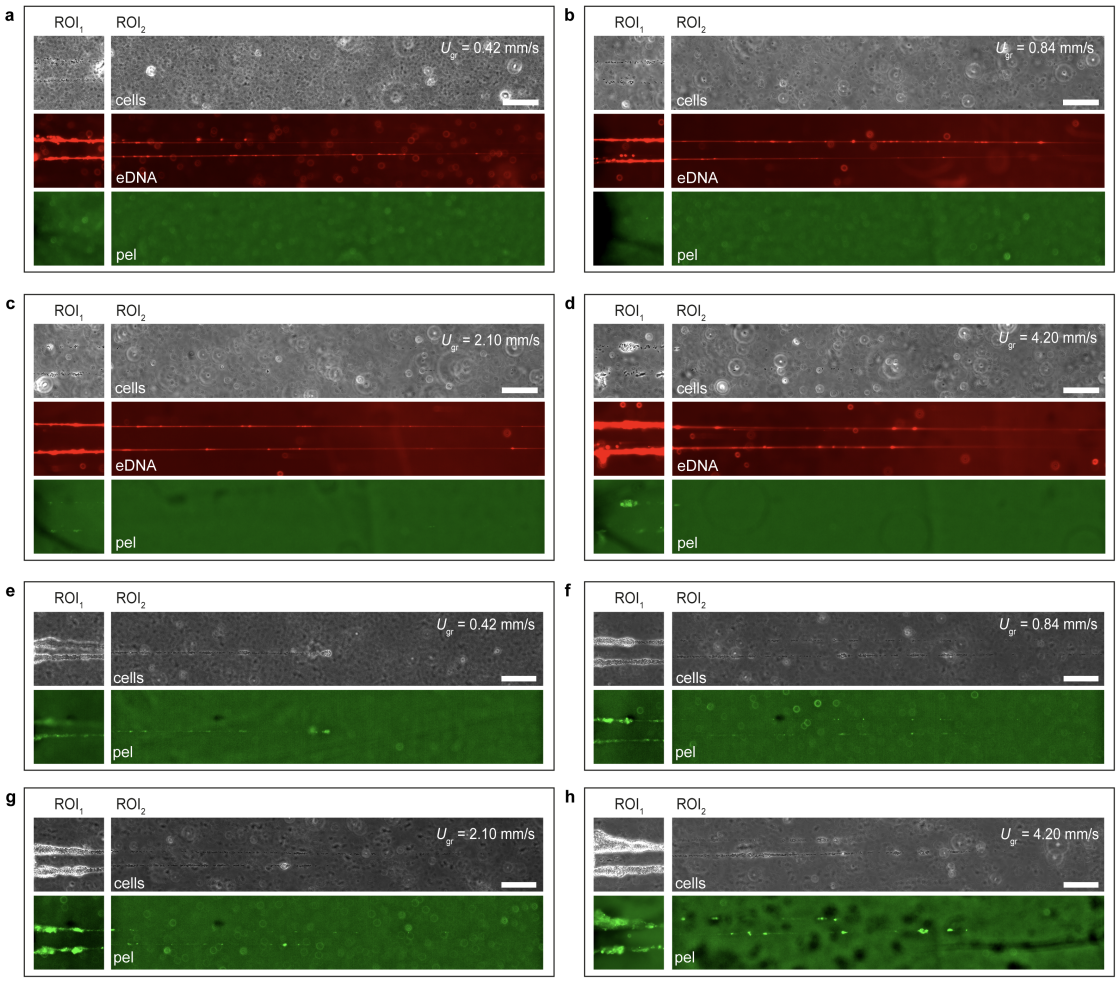

Extended Data Fig. 6 Pel and eDNA distributions along PA14 wild-type and ΔwspF biofilm streamers. **a-d**, Representative phase contrast and fluorescence images of ROI_1 and ROI_2 of PA14 wild-type streamers grown at average flow velocities U_{gr} equal to 0.42 mm/s (a), 0.84 mm/s (b), 2.10 mm/s (c) and 4.20 mm/s (d). The red fluorescence images show the mCherry signal collected from eDNA stained with PI. eDNA constitutes the backbone of the streamers and is detected both in ROI_1 and ROI_2. The green fluorescence images show the GFP signal collected from Pel stained with WFL. Pel is mainly colocalised with the cell aggregates and its abundance in ROI_1 increases with increasing U_{gr}. The increase in Pel secretion by cells subjected to higher flow velocities is consistent with the mechanosensing-driven increase in intracellular c-di-GMP levels [16, 17]. Staining with WFL does not detect Pel in ROI_2 in all flow conditions 5. **e-h**, Representative phase contrast and fluorescence images of ROI_1 and ROI_2 of PA14 ΔwspF streamers grown at average flow velocities U_{gr} equal to 0.42 mm/s (e), 0.84 mm/s (f), 2.10 mm/s (g) and 4.20 mm/s (h). The GFP signal shows that Pel is detected both in ROI_1 and ROI_2. Pel staining was performed on three independent biological replicates for both PA14 wild-type and ΔwspF with consistent results. Overall, Pel staining results are compatible with the inter-strain rheological differences reported in Extended Data Fig. 5

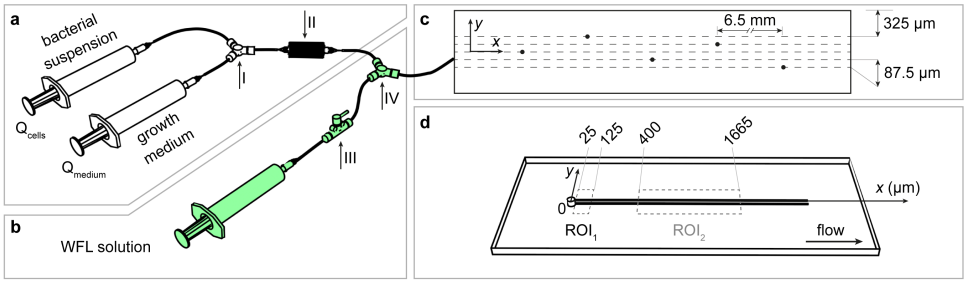

Extended Data Fig. 7 Schematic of the experimental setup. **a**, Setup used to grow biofilm streamers at different U_{gr} and constant flux of cells. The flow rate of the bacterial suspension is $Q_{\mathrm{cells}} = 0.06$ ml/h in all flow conditions. The values of the flow rate Q_{medium} of culture medium used in the different flow conditions are reported in Extended Data Table 1. Only the syringe with the bacterial suspension is used in the channel with the lowest flow rate. The total flow rate values $Q_{\mathrm{gr}} = Q_{\mathrm{cells}} + Q_{\mathrm{medium}}$ during streamer growth in the different flow conditions and the corresponding average flow velocities U_{gr} are reported in Extended Data Table 1. Arrow I indicates the Y connector used to join the streams from the two syringes. Arrow II indicates the straight connector used to homogenise the sample before the channel inlet. **b**, Additional stream used to flow WFL and stain Pel in the matrix of PA14 wild-type and ΔwspF streamers. This flow line is present only in the WFL staining experiments. Arrow III points at the shut-off valve that allow delayed connection of the syringe at $t = 15$ h, preventing overnight degradation of WFL. After imaging of Pel, the WFL syringe is replaced with a syringe containing a PI solution. Arrow IV points at the Y connector used to join the stream from this additional syringe to the main one. **c**, Top-view schematic of the pillar arrangement inside a channel of the microfluidic platform. We modified the arrangement from our previous works [2, 3] to enhance streamer formation. In this work, pillars are not aligned along the centerline of the channel but evenly spaced along the y-axis, with an inter-pillar distance of 87.5 µm. In the current configuration, pillars are evenly spaced along the width of the channel and do not intercept the same flow lines. The distance between the outermost pillars and the channel walls is 325 µm. The distance between pillars in the x direction is 6.5 mm (not in scale in the schematic). 3D COMSOL simulations confirm that the flow field around each pillar is equivalent to that in the original device. **d**, Schematic of two streamers tethered to a micropillar. The dashed rectangles mark ROI_1 and ROI_2.

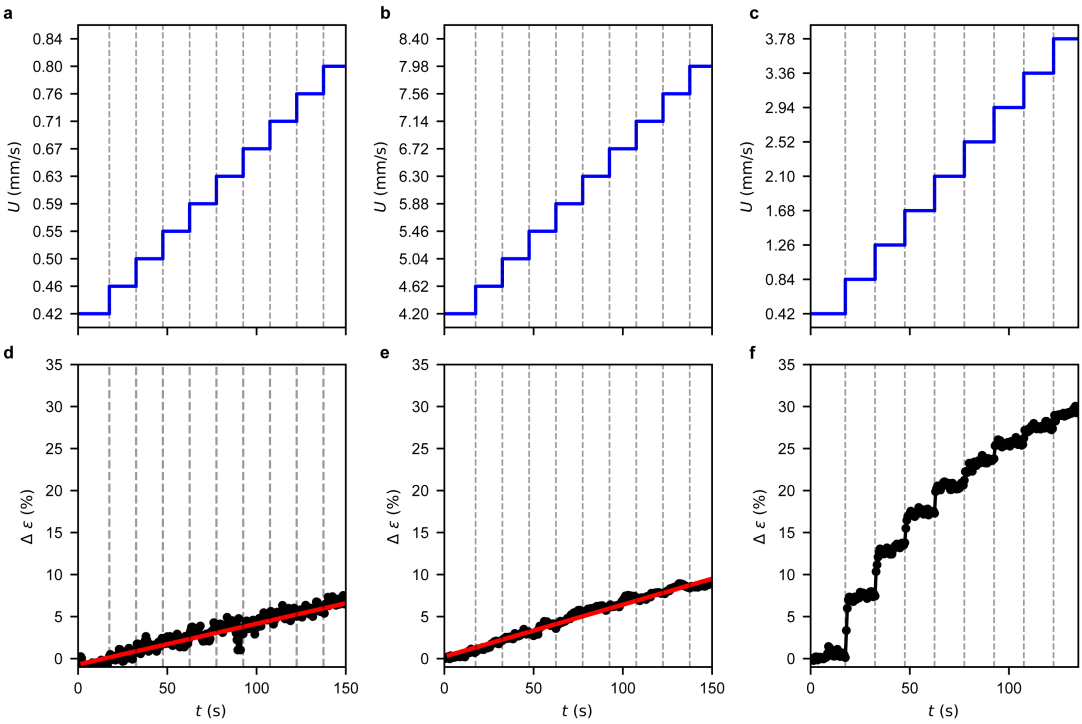

Extended Data Fig. 8 Streamers under prestress σ_0 linearly respond to an axial stress increment $\Delta\sigma = \sigma_0$. **a**, **b**, **d**, **e**, Tests performed to verify that the response of the streamers subjected to an axial stress increment $\Delta\sigma = \sigma_0$ is locally linear in a neighbourhood of σ_0. The average velocity U in the channel is increased from U_{gr} to $2U_{\mathrm{gr}}$ by small steps $\Delta U = U_{\mathrm{gr}}/10$. The time duration of each step is 15 s. Simultaneously, the corresponding strain increment $\Delta\varepsilon$ is measured. Panels **a** and **b** show the average flow velocity inside the microchannel as a function of time during such tests, for the cases $U_{\mathrm{gr}} = 0.42$ mm/s and $U_{\mathrm{gr}} = 4.20$ mm/s, respectively. Panel **d** shows the typical deformation curve measured for a streamer grown at $U_{\mathrm{gr}} = 0.42$ mm/s and subjected to the flow steps in **a**; panel **e** shows the same quantity measured for a streamer grown at $U_{\mathrm{gr}} = 4.20$ mm/s and subjected to the flow steps in **b**. As shown by the linear fits (red lines), the deformation is linear with time, both for this study's lowest and highest flow conditions. This implies that the response of the streamers to the applied axial stress is linear between σ_0 and $\sigma_0 + \Delta\sigma$. **c**, **f** Experiment showing the nonlinear response of a streamer subjected to a stress increment $\Delta\sigma > \sigma_0$. **c** Average velocity U in the channel, increasing from $U_{\mathrm{gr}} = 0.42$ mm/s to $9U_{\mathrm{gr}}$ by steps with magnitude $\Delta U = U_{\mathrm{gr}}$. The time duration of each step is 15 s. **f** The corresponding steps in strain increment $\Delta\varepsilon$ decrease with increasing σ, showing that the response of the streamer to the applied axial stress is nonlinear when $\Delta\sigma > \sigma_0$. The decreasing magnitude of the steps of the strain increment $\Delta\varepsilon$ with increasing σ clearly demonstrates the stress-hardening behaviour of the streamer.

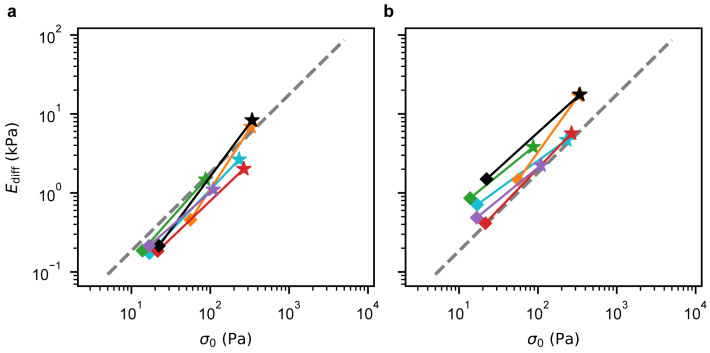

Extended Data Fig. 9 Effects of fluid-structure interaction on the stress hardening behaviour of PA14 wild-type steramers. **a**, Data reported in 3b; each colour identifies two sequential tests related to a same streamer. **b**, Data of panel **a** calculated accounting for the effect of fluid-structure interaction (FSI), following the iterative scheme presented in [2]. The scheme was arrested at the first iteration since higher-order iterations have a negligible effect on the FSI correction, as shown in [2]. The sequential tests in panel **a** have an average slope 1.15 ± 0.10, while the ones in panel **b** 0.95 ± 0.10. The dashed grey lines in panels **a** and **b** show the fit of the data reported in Fig. 3b, with power-law behaviour $\sigma^{0.99}$. These data show that correcting for FSI does not significantly impact the stress-hardening behaviour measured in our experiments.

Extended Data Table 1 Flow parameters for the four channels of the microfluidic platform, used to simultaneously test streamer growth under different flow conditions. The same bacterial batch is used across all channels to minimise biological variability. Q_{cells} is the flow rate of the bacterial suspension, Q_{medium} is that of the culture medium, and Q_{gr} is the total flow rate inside the channel. The average flow velocity is calculated as $U_{\mathrm{gr}} = Q_{\mathrm{gr}}/\mathrm{HW}$, where $\mathrm{H} = 40\,\mu\mathrm{m}$ and $\mathrm{W} = 1000\,\mu\mathrm{m}$ are the channel height and width, respectively. The Reynolds number Re for each condition is calculated as $\mathrm{Re} = \rho U_{\mathrm{gr}}\mathrm{D}$, where ρ is the density of water, and $\mathrm{D} = 50\,\mu\mathrm{m}$ is the pillar diameter.

	Q_{cells} (ml/h)	Q_{medium} (ml/h)	Q_{gr} (ml/h)	U_{gr} (mm/s)	Re (−)
channel 1	0.06	0.00	0.06	0.42	0.02
channel 2	0.06	0.06	0.12	0.84	0.04
channel 3	0.06	0.24	0.30	2.10	0.10
channel 4	0.06	0.54	0.60	4.20	0.20

Supplementary information

Stress-hardening behaviour of biofilm streamers

Giovanni Savorana,[1] Tommaso Redaelli,[1] Domenico Truzzolillo, [2]
Luca Cipelletti, [2,3] Eleonora Secchi [1*]

[1]Department of Civil, Environmental and Geomatic Engineering,
ETH Zurich, Zurich, Switzerland
[2]Laboratoire Charles Coulomb (L2C), Université Montpellier, Montpellier, France
[3] Institut Universitaire de France, Paris, France

*To whom correspondence should be addressed; E-mail: esecchi@ethz.ch.

Elastic stress-hardening behaviour of a DNA network under uni-axial extension

To investigate the origin of the stress-hardening elasticity of the streamers, we compared the power law behaviour observed in our experiments (Fig. 1a, 4i) with the behaviour expected for a 3D network of DNA molecules under uni-axial extension. We describe the force-extension curve of single DNA molecules constituting the network with the following worm-like chain interpolated formula [1], which takes into account the entropic contribution to DNA elasticity:

$$f = \frac{k_{\mathrm{B}}T}{4A}\left[4z + \frac{1}{(1-z)^2} - 1\right], \tag{1}$$

where z is the extension ratio of the molecule, A is the persistence length of DNA , k_{B} is the Boltzmann's constant and T is the temperature. The extension ratio is defined as $z = r/L$, where r is the end-to-end distance of the DNA molecule and L_c its contour length. The free energy W of the DNA molecule subjected to such a force can be calculated by integrating equation 1:

$$W = \frac{k_{\mathrm{B}}TL_c}{4A}\left[2z^2 + \frac{1}{1-z} - z\right] + W_0, \tag{2}$$

where W_0 is a constant [2]. This single-molecule free energy can be used to find the three-dimensional free energy of a network of chains, employing the eight-chain model developed in [3]. This model assumes that a microscopic cube element of a network with edge a_0 has a cross-link in the centre and eight chains extending from the cross-link to the eight corners of the cube. This description assumes that the network is isotropic in the unstrained state, and is equivalent to averaging the contribution of a single chain over eight spatial orientations. This allows finding a relation between the end-to-end distance r of the chains within the network and the invariants of the Cauchy strain tensor, describing the macroscopic state of deformation of the network. In the unstrained state, the end-to-end distance of each chain is $r_0 = \sqrt{N}l = a_0\sqrt{3}/2$, where N is the number of freely jointed segments of length l in a chain between neighbouring cross-links. For an arbitrary strained state where the edges of the microscopic cube are $a_i = a_0\,\lambda_i$ $(i = x, y, z)$, the r of each chain is:

$$r = \frac{a_0}{2}\sqrt{\lambda_1^2 + \lambda_2^2 + \lambda_3^2} = \frac{r_0}{\sqrt{3}}\sqrt{I_1} = l\sqrt{\frac{NI_1}{3}}, \tag{3}$$

where $I_1 = \lambda_1^2 + \lambda_2^2 + \lambda_3^2$ is the first invariant of the Cauchy strain tensor and λ_1, λ_2 , λ_3 are the principal stretches. By substituting eq. 3 into 2, the three-dimensional free energy of a molecule within the network takes the form:

$$W = \frac{k_{\mathrm{B}}TNl}{4A}\left[\frac{2I_1}{J_0} + \frac{\sqrt{J_0}}{\sqrt{J_0} - \sqrt{I_1}} - \sqrt{\frac{I_1}{J_0}}\right] + W_0, \tag{4}$$

where $J_0 = 3N$ [2]. This energy is the contribution of a single worm-like chain within the network. Thus, the energy of the whole network is obtained by mutiplying eq. 4 by the number of chains

per unit volume n:

$$W = n\frac{k_{\mathrm{B}}TNl}{4A}\left[\frac{2I_1}{J_0} + \frac{\sqrt{J_0}}{\sqrt{J_0}-\sqrt{I_1}} - \sqrt{\frac{I_1}{J_0}}\right] + nW_0, \tag{5}$$

In the case of uni-axial extension, assuming network incompressibility, the principal stretches are:

$$\lambda_1 = \lambda,\ \lambda_2 = \lambda_3 = \frac{1}{\sqrt{\lambda}}, \tag{6}$$

where λ is the stretch ratio in the direction of extension. Therefore, the first invariant is:

$$I_1 = \lambda^2 + \frac{2}{\lambda}. \tag{7}$$

In this case, the true stress (calculated with respect to the deformed cross section) in the direction of extension is [2]:

$$\begin{aligned}\sigma &= 2\left(\lambda^2\frac{\partial W}{\partial I_1} - \frac{1}{\lambda}\frac{\partial W}{\partial I_1}\right) = \\ &= n\frac{k_{\mathrm{B}}TNl}{4A}\left(\lambda^2 - \frac{1}{\lambda}\right)\left(\frac{4}{J_0} + \frac{\lambda\sqrt{J_0\lambda}}{(\sqrt{J_0\lambda}-\sqrt{\lambda^3+2})^2\sqrt{\lambda^3+2}} - \frac{\sqrt{\lambda}}{\sqrt{J_0(\lambda^3+2)}}\right).\end{aligned} \tag{8}$$

Due to the finite chain extensibility, the stress diverges when $\lambda \to \lambda^*$, where λ^* is the stretch ratio such that

$$\lambda^{*3} - J_0\lambda^* + 2 = 0. \tag{9}$$

From equation 8, the differential Young's modulus E_{diff} of the network can be obtained as [4]:

$$E_{\mathrm{diff}} = \lambda\frac{\mathrm{d}\sigma}{\mathrm{d}\lambda}. \tag{10}$$

From equations 8 and 10 it is then possible to obtain the functional relation between E_{diff} and σ for a network under uni-axial extension (Fig. 4i). This shows a plateau for small values of σ, corresponding to the linear elastic response of the network, and region at large σ where $E_{\mathrm{diff}} \propto \sigma^{1.5}$. When the network is such that the number N of freely jointed segments between neighbouring cross-links is high enough ($N > 100$), the model predicts a cross-over regime for intermediate values of σ where $E_{\mathrm{diff}} \propto \sigma$, as observed for the streamers.

For a network of DNA molecules ($A \approx 50\,\mathrm{nm}$ [1]) at room temperature ($T = 293\,\mathrm{K}$), the cross-over regime overlaps the prestress regime spanned in the sequential tests (Fig. 4i) when considering $N \geq 1000$ and chain density between $n = 5\times10^{20}\,\mathrm{m}^{-3}$ and $n = 1\times10^{21}\,\mathrm{m}^{-3}$. The largest density value corresponds to the maximum density of DNA chains with radius $R_{\mathrm{DNA}} = 0.0024\,\mu\mathrm{m}$ [5] and length equal to $L_c = Nl = 50\,\mu\mathrm{m}$, with $N = 1000$ and the length l of a single freely jointed segment chosen as $l = A = 50\,\mathrm{nm}$, satisfying the condition $l \leq A \leq L_c$ [2].

References

[1] Bustamante, C., Marko, J. F., Siggia, E. D. & Smith, S. Entropic elasticity of lambda-phage DNA. *Science* **265**, 1599–1600 (1994).

[2] Ogden, R. W., Saccomandi, G. & Sgura, I. On worm-like chain models within the three-dimensional continuum mechanics framework. *Proc. R. Soc. A: Math. Phys. Eng. Sci.* **462**, 749–768 (2006).

[3] Arruda, E. M. & Boyce, M. C. A three-dimensional constitutive model for the large stretch behavior of rubber elastic materials. *Journal of the Mechanics and Physics of Solids* **41**, 389–412 (1993).

[4] Scott, N. The incremental bulk modulus, young's modulus and poisson's ratio in nonlinear isotropic elasticity: Physically reasonable response. *Mathematics and Mechanics of Solids* **12**, 526–542 (2007).

[5] Mugunthan, S. *et al.* RNA is a key component of extracellular DNA networks in *Pseudomonas aeruginosa* biofilms. *Nat. Commun.* **14**, 7772 (2023).